[Research Paper] 대한금속 · 재료학회지 (*Korean J. Met. Mater.*), Vol. 60, No. 2 (2022) pp.141-148
DOI: 10.3365/KJMM.2022.60.2.141

Sintering Mechanism and Enhanced Piezoelectric and Crystal Structural Properties of (1-x)Ba($Zr_{0.2}Ti_{0.8}$)O_3-x($Ba_{0.7}Ca_{0.3}$)TiO_3 Lead Free Ceramics

Yoo-Young Oh[1], Gwangseop Lee[2], Masao Kamiko[3], and Jung-Hyuk Koh[1,2,*]

[1]*School of Electrical and Electronics Engineering, Chung-Ang University, Seoul 06974, Republic of Korea*
[2]*Department of Intelligent Energy and Industry, Chung-Ang University Seoul 06974, Republic of Korea*
[3]*Institute of Industrial Science, The University of Tokyo, Tokyo 113-8668, Japan*

Abstract: A lead-free piezoelectric ceramic, (1-x)Ba($Zr_{0.2}Ti_{0.8}$)O_3-x($Ba_{0.7}Ca_{0.3}$)TiO_3 (hereafter (1-x)BZT-xBCT), was investigated for functional device applications. Lead-free piezoelectric materials with high piezoelectric charge coefficients and voltage coefficients are indispensable for functional industrial applications. Piezoelectric ceramic specimens tend to shrink in size during the sintering process without melting. This study focused on this phenomenon as a unique characteristic of piezoelectric ceramic materials, and derived the materials' activation energies from this phenomenon, employing the Arrhenius relationship. Then the estimated activation energy was employed to determine the relationship between the piezoelectric properties and crystalline properties, while varying sintering temperature and chemical stoichiometric composition. Piezoelectric properties can change depending on the sintering temperature and process conditions. Crystalline properties and piezoelectric properties can be influenced by the sintering temperature and holding times. In this research, sintering temperature dependent structural and dielectric properties were investigated. (1-x)BZT-xBCT ceramics showed the highest piezoelectric coefficient of 470 pC/N. Sintering temperature dependent shrinkage rate and activation energy were estimated and calculated for the various sintering processes. In this research, two different activation energies for the shrinkage process were estimated.

(Received March 11, 2021; Accepted October 28, 2021)

Keywords: piezoelectric material, (1-*x*)Ba($Zr_{0.2}Ti_{0.8}$)O_3–*x*($Ba_{0.7}Ca_{0.3}$)TiO_3, shrinkage mechanism, activation energy

1. Introduction

Lead-based piezoelectric materials have been intensively investigated for their excellent piezoelectric (pC/N) and inverse piezoelectric (pm/V) properties. As a representative piezoelectric material, (Pb,Zr)TiO_3 has been extensively employed in industrial applications due to its excellent piezoelectric and mechanical properties (d_{33} ~ 360 pC/N, k_p ~ 0.51) with high Curie temperature (> 300 ºC) [1-3]. Accordingly, this material has been tested for various applications including actuators, sensors and transducers, which can be used in conditions of heavy load and mechanical force. Despite these excellent mechanical and piezoelectric properties, lead based piezoelectric materials also present environmental issues due to the toxic and harmful properties of lead. To avoid these environmental problems, lead free alternatives to replace lead-based piezoelectric materials have been widely and intensively investigated. Among them $Bi_{0.5}Na_{0.5}TiO_3$ (BNT), $Na_{0.5}K_{0.5}NbO_3$ (NKN) and $BaTiO_3$ (BT) are representative lead-free piezoelectric materials. NKN has a high piezoelectric charge coefficient of 160 pC/N with a high Curie temperature of 420 ºC [4,23]. But NKN has the drawback of being highly volatile because of the low melting temperatures of Na and K [5]. Another alternative lead-free piezoelectric material candidate, BNT, has a very high piezoelectric charge coefficient 230.8 pC/N, a relatively larger electromechanical coupling factor (k_p ~ 0.41), larger remanent polarization (P_r ~ 40 μC/cm^2) and a better *P–E* hysteresis loop at relatively high temperature then other lead-free piezoelectric ceramics

- 이광섭: 석사과정, 오유영: 석사, 고중혁 · Masao Kamiko: 교수
**Corresponding Author:* Jung-Hyuk Koh
[Tel: +82-2-820-5311, E-mail: jhkoh@cau.ac.kr]

[6-7]. However, its open stress vs strain curve means applied energy can accumulate, resulting in high fatigue and lower reliability [8]. BT has shown promising properties, including a high piezoelectric charge coefficient of more than 460 pC/N [9-10]. Therefore, in this research, a substitution type of BT material was selected to investigate the relationship between activation energy and piezoelectric properties.

Piezoelectric ceramics have typically been fabricated with high density to achieve a high d_{33} and reliable mechanical stability. In this paper, the activation energy of BZT-BCT was derived from its shrinking behavior during the sintering process, and the sintering temperature and BCT contents ($0.4 \leq x \leq 0.5$) were optimized. The Arrhenius equation was adopted to derive activation energy from shrinking behavior. $(1-x)Ba(Zr_{0.2}Ti_{0.8})O_3$-$x(Ba_{0.7}Ca_{0.3})TiO_3$ has been intensively investigated for application in sensors and energy harvester because of its high piezoelectric performance and properties [19-20]. A high piezoelectric charge coefficient d_{33} of 620 pC/N has been reported, and $(1-x)Ba(Zr_{0.2}Ti_{0.8})O_3$–$x(Ba_{0.7}Ca_{0.3})TiO_3$ (hereafter BZT-BCT) piezoelectric ceramics have been investigated to replace PZT lead based piezoelectric materials [15]. One important feature of BZT-BCT is that the R-T phase transition is expected to occur between BCT contents of $0.4 \leq x \leq 0.5$. It is known that the phase transition leads to high piezoelectric performance in materials such as PZT and PMN-PT [15,18,19,22].

In this study, we have focused on (1-*x*)BZT–*x*BCT materials with $x(Ba_{0.7}Ca_{0.3})TiO_3$ contents of $x = 0.4$, 0.425, 0.45, 0.475, 0.5 and sintering temperatures of 1475 ºC, 1500 ºC, and 1525 ºC. This study has focused on the shrinkage mechanism and activation energy of BZT-BCT ceramics to explain its outstanding piezoelectric properties. The densification behavior of BZT-BCT and its microscopic surface were also measured.

2. Experimental

2.1 Fabrication process of (1-x)BZT-xBCT

First, stoichiometric mixtures of (1-*x*)BZT–*x*BCT ($x = 0.4$, 0.425, 0.45, 0.475, 0.5) ceramic were sintered by conventional solid state sintering process. Powders of $BaCO_3$(purity 99.9%, Sigma-Aldrich Co., Ltd.), TiO_2(purity 99.9%, Kojundo), ZrO_2(purity 99.0%, Sigma-Aldrich Co. Ltd.), and $CaCO_3$ (purity 99.0%, Sigma-Aldrich Co., Ltd.), were mixed with ethyl alcohol and ball milled for 24h. After the drying process, powders of the (1-*x*)BZT-*x*BCT ceramics were calcined at 1350 ºC for 2h. The calcination process is essential to eliminate un-desirable substances such as carbides. After the calcination process, partly aggregated powders were smashed and re-powdered again to enhance their crystallization during the sintering process. Sintering can be used to improve crystalline structure. Although these calcination and sintering processes have different purposes, portions of their processing temperature range overlap. However, if the calcined powders are re-powdered before the sintering process, the calcination will not significantly affect the sintering process. This indicates the calcination process does not affect the activation energy induced by shrinking behavior.

Green bodies were pressed into disks under 3 metric tons (12 mm in diameter and 1.6mm in thickness). To investigate the shrinkage mechanism of (1-*x*)BZT-*x*BCT ceramics, specimens were sintered at various temperatures ranging from 800 ºC - 1525 ºC, with a holding time of 3 h and a heating rate and cooling rate of 3 ºC/min [16-17]. The relative shrink ratios of the (1-*x*)BZT-*x*BCT samples were measured by hydrometer, and then the samples were thermally etched for 10 min to investigate their surface morphologies using field emission scanning electron micrography. The crystalline structure of each specimen was investigated using X-ray diffraction (D8-Advance/Bruker-AXS) analysis. The relative dielectric constant (ε_r) was measured by impedance analyzer (Agilent 4294A). The relative density was measured using the Archimedes method. The volume was calculated as the product of the area and thickness of the fabricated sample. Thorough shrinkage tests of each of these samples were conducted at various sintering temperatures.

2.2 Mathematical method; Arrhenius equation

Firstly, the kinetic equation was plotted, which is the relative shrinkage ratio with exponent n versus the reciprocal of T to derive the relation between shrinkage ratio and activation energy in equation (1), where L is the volume after the sintering process, and L_0 is the volume before the sintering process. K is the rate constant and T is the absolute

temperature.

$$\left(\frac{L-L_0}{L_0}\right)^n = \frac{Kt}{T}, \quad (1)$$

Then Eq. (2) is replotted to get exponent n. In this replotted equation, t is the holding time of the sintering process.

$$ln\left(\frac{L-L_0}{L_0}\right) = \frac{1}{n}ln\left(\frac{K}{T}\right) + \frac{1}{n}ln(t), \quad (2)$$

Eq. (3) can be derived from Eq. (1) in Arrhenius equation form by differentiation with respect to T, where a is the heating rate.

$$\frac{d\left(\frac{L-L_0}{L_0}\right)}{dT} = \frac{1}{n}T^{-1}a^{-\frac{1}{n}} \bullet K^{\frac{1}{n}}, \quad (3)$$

K can be rearranged by the relationship between activation enegy Q, gas constant R (R = 8.314 J/Kmol).

$$K = K_0 e^{-\frac{Q}{RT}}, \quad (4)$$

By re-arranging Equation (1), Equation (3) and Equation (4), Equation (5) can be derived

$$ln\left\{T\left[\frac{d(L-L_0)}{dT}\right]\right\} = ln\left(\frac{1}{n} \bullet K_0^{\frac{1}{n}}\right) - \frac{1}{n}ln(a) - \frac{Q}{nRT}, \quad (5)$$

3. Results and Discussion

Figure 1 shows the relative shrinkage ratio of the (1-x) BZT–xBCT ceramics sintered at temperatures from 800 °C to 1525 °C. As shown in the figure, the porosity of the ceramic can be decreased during the sintering process without melting. After the sintering process, the relative shrinkage ratios of the (1-x)BZT–xBCT ceramics were measured. As shown in Figure 1, the (1-x)BZT–xBCT ceramics started to shrink at 1200 °C. The BCT sample with a content of 0.5 showed the highest shrinkage ratio in the temperature range of 800 °C -1200 °C, and the sample with the BCT content of 0.475 showed the highest shrinkage ratio in the temperature range of 1200 °C - 1525 °C. The sintering process of the (1-x)BZT–xBCT ceramics was completed near 1500 °C. The shrinkage rate of (1-x)BZT–xBCT was around 31.1% - 34.2 % at a sintering temperature of 1500 °C.

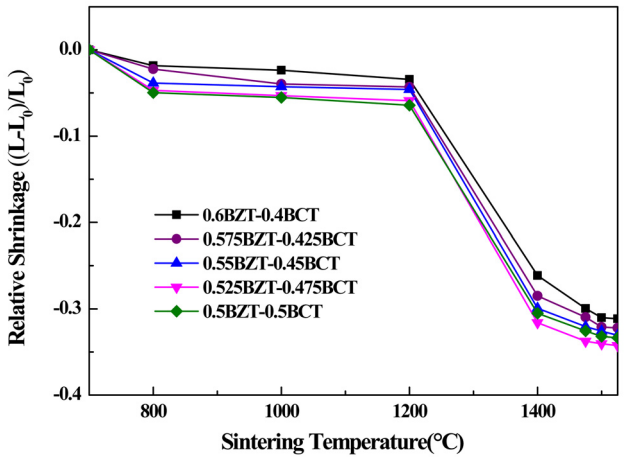

Fig. 1. Relative shrinkage ratio of (1-*x*)Ba($Zr_{0.2}Ti_{0.8}$)O_3-*x*($Ba_{0.7}Ca_{0.3}$)TiO_3 ceramics for different sintering temperature.

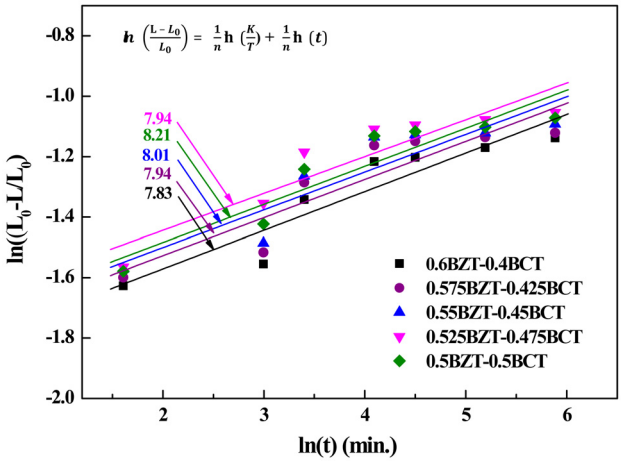

Fig. 2. Isothermal shrinkage curves of (1-*x*)Ba($Zr_{0.2}Ti_{0.8}$)O_3-*x*($Ba_{0.7}Ca_{0.3}$)TiO_3 depending on the holding time.

Figure 2 shows the isothermal shrinkage curves of the (1-x) BZT–xBCT ceramics depending on holding time. Different holding times were analyzed using the kinetic equation [12-13]. Also, different sintering time depending on the sintering temperature was investigated.

Eq. (2) was employed to plot the $ln\left(\frac{L-L_0}{L_0}\right)$ vs ln(t) data depending on the holding time. The exponent of n can be calculated from the slopes (1/n) of the straight line fitted by the isothermal shrinkage in Figure 2. n can be related to material properties and the different shrinkage rates of the sintered materials. As a result, the values of n were determined to be 7.83, 7.94, 8.01, 7.94 and 8.21 for the (1-*x*)BZT–*x*BCT ceramics, respectively. The different exponent n indicates that each specimen has a distinctive shrinking behavior, which also leads to their having their own distinct activation energy.

Figure 3 shows the activation energy of the (1-x)BZT–xBCT ceramics, simulated using the temperature dependent

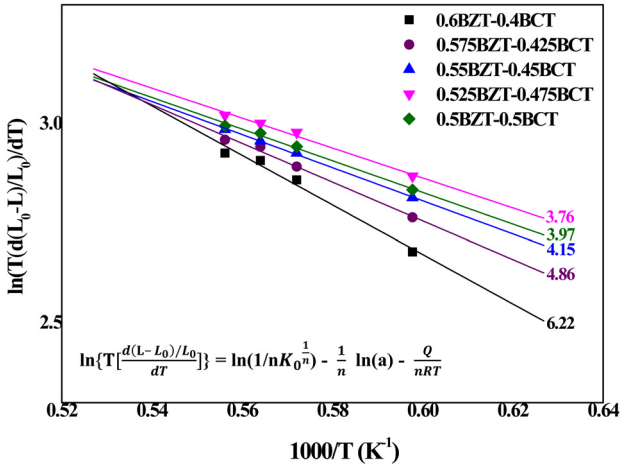

Fig. 3. Reconstructed curves for the relative shrinkage ratio (1-*x*)Ba($Zr_{0.2}Ti_{0.8}$)O_3-*x*($Ba_{0.7}Ca_{0.3}$)TiO_3 sintered from 1400 to 1525 °C.

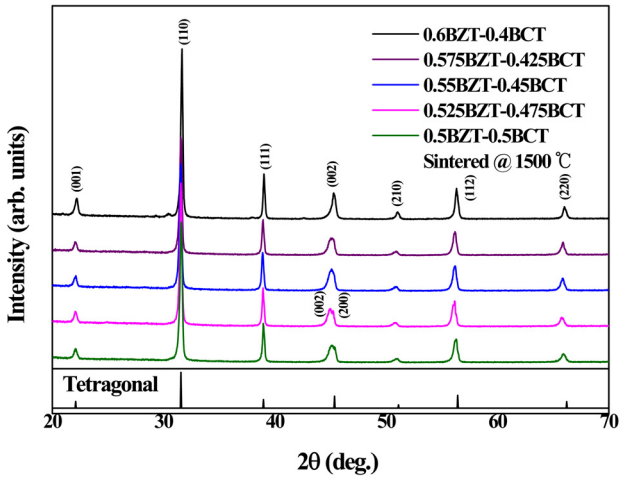

Fig. 4. X-ray diffraction patterns of (1-*x*)Ba($Zr_{0.2}Ti_{0.8}$)O_3-*x*($Ba_{0.7}Ca_{0.3}$)TiO_3 ceramics sintered at 1500 °C.

shrinkage rate from Figure 1. Figure 3 shows the reconstructed curves for the relative shrinkage ratio of (1-x)BZT–xBCT samples sintered at 1400 to 1525 °C which is translated to Arrhenius equation form. Inverse temperature versus shrinkage rate gives the activation energy from the slope in Figure 1. Since the calcination process was carried out at 1350 °C, lower than the 1300 °C sintering temperature, the shrinkage ratio was not considered in calculating the shrinkage mechanism. As a result, from the slope (Q / nRT) of the ln $T\left[\frac{d(L-L_0)/L_0}{dT}\right]$ versus 1/T equation, the activation energy for the sintering process can be calculated from the slope in Figure 2.

The calculated activation energies Q in the temperature range 1400 - 1525 °C were around 404.9, 320.8, 276.3, 248.2 and 270.9 kJ/mol, respectively.

Table 1 lists the exponents of n and activation energies Q of the (1-x)BZT–xBCT ceramics. The lowest n value was 7.83 for the 0.6BZT–0.4BCT ceramic. The activation energy of the specimens means the internal energy needed to grow grains during the sintering process. Therefore, the lowest activation energy leads to the most easily sintered sample, compared with other specimens [12-14].

Figure 4 shows the X-ray diffraction θ-2θ patterns of the (1-x)BZT–xBCT ceramics sintered at 1500 °C., to investigate their crystalline properties The patterns indicate that all the specimens are single-phase. Samples with BCT contents of $0.4 \leq x \leq 0.45$ exhibited a rhombohedral structure. As shown in the figure, the split peak of (002)/(200) at BCT contents (x) of $0.475 \leq x \leq 0.5$ indicate a tetragonal structure, which is the phase transition region between the rhombohedral phase and tetragonal phase [19]. Therefore, x approaching $x = 0.45$ (1-x)BZT–xBCT ceramics have a mixed phase of rhombohedral and tetragonal structures.

Moreover, the Bragg reflections of the (002)/(200) planes showed that the position of the (002) peak shifted to a slightly lower angle when the BCT content was increased from 0.4 to 0.475, then shifted to a higher angle at a BCT content of 0.5. The (002) peak shift to a lower angle means that the volume of the (1-x)BZT–xBCT ceramics increased, since the two different rhombohedral and tetragonal phases are mixed near $x = 0.45$. But when the BCT contents were increased further to $x = 0.475$, the (002)/(200) planes moved to a higher position. This means the volume of the (1-x)BZT–xBCT ceramics decreased. The atomic radius of Ba

Table 1. The values of n and the activation energy Q.

BCT[*x*]		0.4	0.425	0.45	0.475	0.5
n		7.83	7.94	8.01	7.94	8.21
Q [kJ /mol]	1200~1525[°C]	404.91	320.82	276.36	248.21	270.98

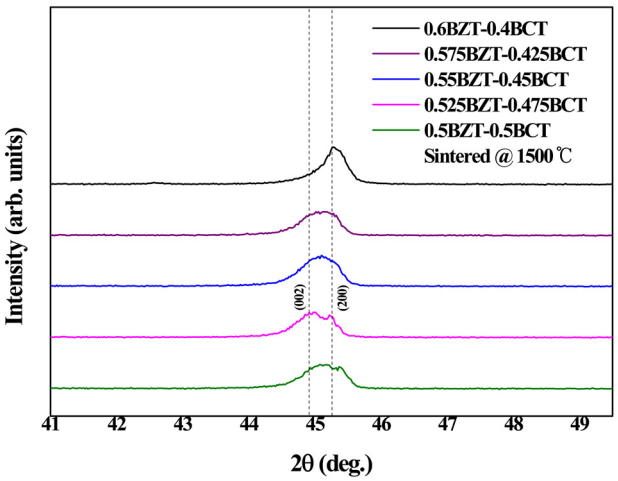

Fig. 5. Enlarged X-ray diffraction patterns (002) and (200) plane of (1-*x*)Ba($Zr_{0.2}Ti_{0.8}$)O_3-*x*($Ba_{0.7}Ca_{0.3}$)TiO_3 sintered at 1500 °C.

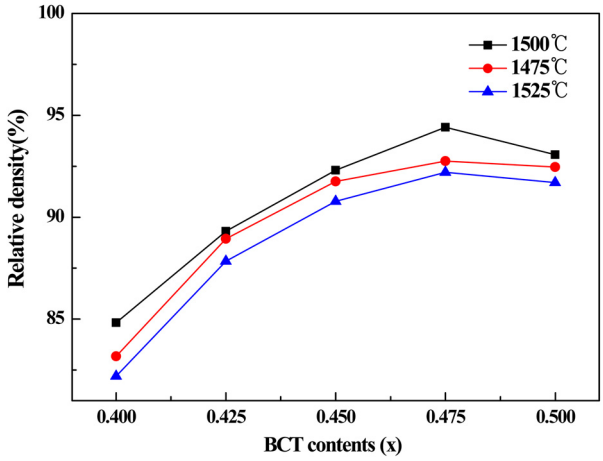

Fig. 6. Relative density of (1-*x*)Ba($Zr_{0.2}Ti_{0.8}$)O_3-*x*($Ba_{0.7}Ca_{0.3}$)TiO_3 ceramics for sintering temperature of 1475, 1500, 1525 °C.

and Zr are sligthly larger than those of the Ca and Ti atoms. As the x composition increased, Ba and Zr content decreased, while Ca and Ti were increased. This has the effect of decreasing the volume of the (1-x)BZT–xBCT structure. The atomic radius of Ba, Zr, Ca, Ti are 1.43, 1.06, 0.87, and 0.64 Å, respectively.

The position of the (002) peak at 45.02° relative to that that the lattice constant c of the 0.525 BZT–0.475BCT implies it has increased relative to that of the other specimens. In fact, the 0.525 BZT–0.475BCT had the highest c lattice parameter among all specimens.

Figure 5 shows the enlarged X-ray diffraction pattern in the range of 43 to 46.5, where the (002) and (200) planes exist. The symetric shape near 2θ = 45°, for BCT contents of $0.4 \leq x \leq 0.45$, indicate a single rhombohedral structure, while the split peak of (002)/(200) planes indicate that BCT contents of 0.475, 0.5 have a rhombohedral with tetragonal structure. This represents a peak shift of (002) in the (1-x)BZT–xBCT ceramics. As shown in the figure, 0.525BZT–0.475BCT show a split peak for the (002) and (200) planes, indicating increased tetragonality. When the composition of x = 0.425, 0.45, and 0.475, the peak positions were very similar. However, when the BCT contents were 0.5, then the (002) peak was shifted to a higher angle as the composition of the BCT was increased. In the tetragonal structure, increased (002) peaks means that Ba, Zr, which have larger ionic radii compared to Ca, Ti, decreased as the BCT contents increased, reducing the lattice parameter according to Bragg's law. Also, when x = 0.4, 0.425, the rhombohedral structure peak was shifted to a lower angle. According to the crystal geometry equation, α approaches 90 degrees, and an increase in the unit cell volume can be seen.

Figure 6 shows the relative densities of the (1-x)BZT–xBCT samples sintered at 1475 °C, 1500 °C, 1525 °C. All sintering temperature showed that relative density increased up to BCT contents of about x = 0.475 with 94.4%, and then decreased. This density increase likely indicates the optimum BCT content and sintering temperature. In addition, this bulk density is probably related to the degree of crystalization in the (1-x)BZT–xBCT ceramics. Because the crystalization process is related to the BCT contents and sintering temperature, the relative density is also related to BCT contents.

As the sintering temperature was increased from 1475 to 1500 °C, the crystalization process progressed due to its low activation energy, as discussed in Figure 3. However, when the sintering temperature was further increased above 1500 °C, the volume increased and weight might be decreased due to the low evaporation temperature of Ca, at 1484 °C. The BZT-BCT material exhibited tricritical points in the phase diagram, and near the tricritical points the x = 0.475 phase can be drastically changed. With increasing BCT content, the BZT-BCT material forms rhombohedral, orthorombic, and tetragonal structures. Due to this phase transition, relative density increased up to the tricritical points

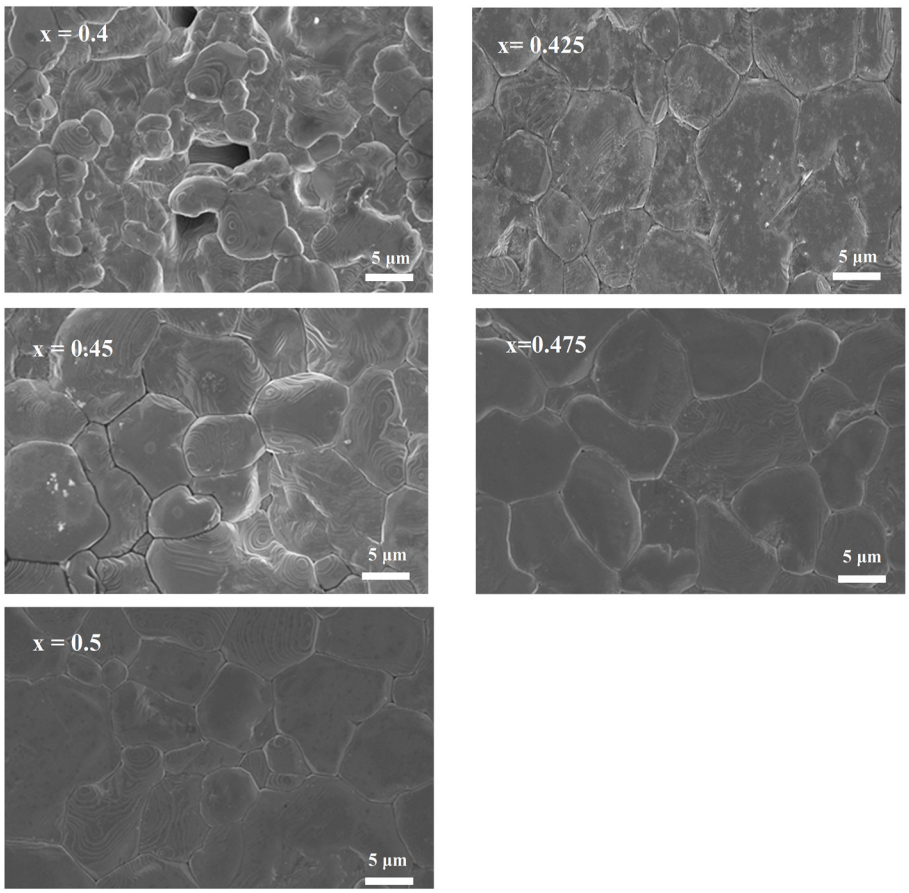

Fig. 7. Field Emission Scanning Electron Microscopy micrographs of the (1-*x*)Ba($Zr_{0.2}Ti_{0.8}$)O_3-*x*($Ba_{0.7}Ca_{0.3}$)TiO_3 ceramics for sintering temperature of 1500 °C.

at x = 0.475. However, relative density can be decreased due to the phase transition with mixed phase [16].

Figure 7 shows Field emission scanning electron microscopy micrographs of the thermally etched (1-x)BZT–xBCT ceramics sintered at 1500 °C. The (1-x)BZT–xBCT ceramic has an average grain size of 9.5-11 μm. As shown in Fig. 7(a), 0.6BZT–0.4BCT has a porous morphological surface, explaining the lower piezoelectric charge coefficient. With increasing BCT content, the grain size becomes larger with a clearer grain boundary, supporting the data in Figure 6, showing the bulk density of the (1-x)BZT–xBCT ceramics. For 0.525BZT–0.475BCT the minimum activation energy needed to grow grains was assumed to be 201.88 kJ/mol, in the temperature range of 1200 °C - 1525 °C, resulting in a dense, coarse-grain microstructure, while 0.6BZT–0.4BCT needed the highest activation energy, 561.6468 kJ/mol, at a temperature range of 1200 °C - 1525 °C, producing a fine, porous-grain microstructure.

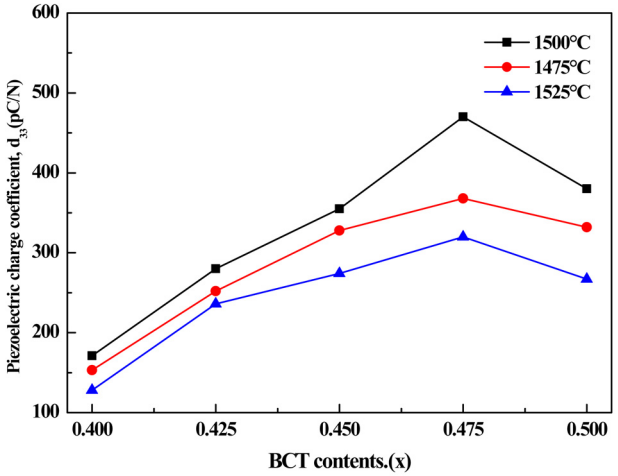

Fig. 8. Piezoelectric charge coefficient of (1-x)Ba($Zr_{0.2}Ti_{0.8}$)O_3-x($Ba_{0.7}Ca_{0.3}$)TiO_3 ceramics for sintering temperature of 1475 °C, 1500 °C, 1525°C.

Figure 8 displays the piezoelectric charge coefficients of

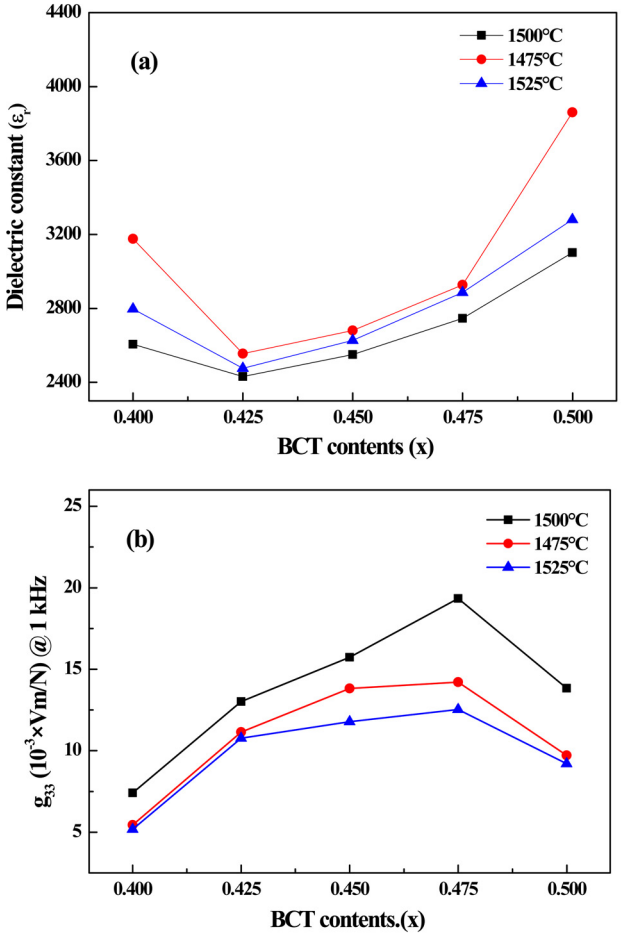

Fig. 9. (a) Dielectric constant and (b) Piezoelectric Voltage constant coefficient of (1-*x*)Ba($Zr_{0.2}Ti_{0.8}$)O_3-*x*($Ba_{0.7}Ca_{0.3}$)TiO_3 ceramics for sintering temperature of 1475 °C, 1500 °C, 1525 °C at 1 kHz.

(1-x)BZT–xBCT samples sintered at 1475 °C, 1500 °C, 1525 °C. As shown in the figure, all of the specimens exhibit an increasing piezoelectric charge coefficient up to 470 pC/N at a BCT content of 0.475, and then decrease. Among other sintering temperatures, the specimens sintered at 1500 °C showed a relatively higher piezoelectric charge constant, indicating that the optimized sintering temperature was 1500 °C from the perspective of energy harvesting.

Figure 9(a) displays the dielectric constants of (1-x)BZT–xBCT at 1kHZ (1475 °C, 1500 °C, 1525 °C). At all sintering conditions the samples exhibited the lowest dielectric constant with BCT contents of 0.425, and then increased with increasing BCT contents. The lowest dielectric constant of (1-x)BZT–xBCT was 2431.95 for the sample sintered at 1500 °C. Fig. 9(b) displays the piezoelectirc voltage constants of (1-x)BZT–xBCT ceramics at 1 kHz (1475 °C, 1500 °C, 1525 °C). The specimens sintered at a temperature of 1500 °C had a relatively higher piezoelectric charge constant specimens then the other sintering temperatures, and showed the highest piezoelectric voltage constant. Also, the sample with the BCT content of 0.475 had the highest piezoelectric voltage constant under all sintering temperature conditions. The highest value was 19.34 mVm/N at a BCT content of 0.475.

4. Conclusions

In this research, the relationship between shrinking behavior, activation energy and the piezoelectric properties of lead-free piezoelectric (1-*x*)Ba($Zr_{0.2}Ti_{0.8}$)O_3–*x*($Ba_{0.7}Ca_{0.3}$)TiO_3 ceramics were investigated. There were two shrinkage mechanisms, located in the temperature ranges of 800-1200 °C and 1200 -1525 °C, respectively. Each specimen had a distinct shrinkage mechanism, defined by exponent n. Among the specimens, those with BCT contents of 0.4 had the lowest value of exponent n, 7.83. With increasing BCT contents up to 0.475, the n value and activation energy decreased. 0.55BZT-0.45BCT exhibited the lowest activation energy of 129.86 kJ/mol in the sintering temperature range of 800 °C-1200 °C and 0.525BZT-0.475BCT showed the lowest activation energy of 248.21kJ/mol in the temperature range of 1200 °C-1525 °C. Also, the low BCT content specimens had a fine porous morphological surface, and with increasing BCT contents, the morphological surface became dense with a coarse grain structure. Based on the investigation of the shrinkage mechanism, the sintering temperature and piezoelectric properties were optimized. The (1-x)BZT–xBCT ceramics (*x* = 0.4. 0.425, 0.45, 0.475, 0.5) sintered at 1500 °C exhibited a relatively high bulk density compared to those sintered at other temperatures. The highest piezoelectric charge coefficient (470 pC/N) and piezoelectric voltage coefficient (19.34 mVm/N) at a frequency of 1 kHz were obtained at the sintering temperature of 1500 °C and BCT content of 0.475.

Acknowledgements

This work was supported by Korea Institute for Advancement

of Technology (KIAT) grant funded by the Korea Government (MOTIE) (P0017308, Global Human Resource Development Program for Industrial Innovation) and supported by Chung-Ang University Research Grant 2020.

REFERENCES

1. Shujun Zhang, Ru Xia, Laurent Lebrun, Dean Anderson, and Thomas R. Shrout, *Mater. Lett.* **59**, 3471 (2005).
2. Yiping Guo, Ken-ichi Kakimoto, and Hitoshi Ohsato, *Mater. Lett.* **59**, 241 (2005).
3. Dong-Jin Shin and Jung-Hyuk Koh, *J. Alloys Compd.* **555**, 390 (2013).
4. D.Q.Xiao, D.M.Lin, J.G.Zhu, and P.Yu, *J. Electroceramics.* **21**, 34 (2008).
5. Zhenhua Luo, Julia Glaum, Torsten Granzow, Wook jo, Robert Dittmer, and Mark Hoffman, *J. Am. Ceram. Soc.* **94**, 529 (2011).
6. Tomoaki Karaki, Kang Yan, Toshiyuki Miyamoto, and Masatoshi Adachi, *Jpn. J. Appl. Phys.* **46**, L97 (2007).
7. Gao Feng, Hong Rongzi, Liu Jiaji, Li Zhen, Cheng Lihong, and Tian Changsheng, *J. Alloys Compd.* **475**, 619 (2009).
8. Dean S. Keeble, Feres Benabdallah, Pam A. Thomans, Mario Maglione, and Jens Kreisel, *Appl. Phys. Lett.* **102**, 092903 (2013).
9. Jinhwan Kim and Jung-Hyuk Koh, *J. Alloys Compd.* **638**, 155 (2015).
10. Wook-Hee Han and Jung-Hyuk Koh, *Ceram. Int.* **44**, 5352 (2018).
11. Satyajit Shukla, Sudipta Seal, Rashmi Vij, and Sri Bandyopadhyay, *Nano. Lett.* **3**, 397 (2003).
12. Wenfeng Liu and Xiaobing Ren, *Phys. Rev. Lett*. **103**, 257602 (2009).
13. Dong-Jin Shin, Jinhwan Kim, and Jung-Hyuk Koh, *J. Eur. Ceram. Soc.* **38**, 4395 (2018).
14. Yang Bai, Ales Matousek Pavel Tofel Vijay Bijalwan, Bo Nan, Hana Hughes, and Tim W. Button, *J. Eur. Ceram. Soc.* **35**, 3445 (2015).
15. B. Noheda, D. E. Cox, and G. Shirane, *Phys. Rev. B* **66**, 054104 (2002).
16. Xiaodong Yan, Mupeng Zheng, Yudong Hou, and Mankang Zhu, *J. Eur. Ceram. Soc.* **37**, 2583 (2017).
17. H. Kaddoussi, A. Lahmar, Y. Gagou, B. Manoun, J.N. Chotard, J.-L. Dellis, Z. Kutnjak, H. Khemakhem, B. Elouadi, M. El Marssi, *J. Alloys Compd.* **713**, 164 (2017).
18. Jie Liu, Bin Yang, Lijun Lu, Xiaolin Wang, Xiuyan Li, Xiang Chen, Jingquan Liu, *Sens. Actuator A Phys.* **303**, 111796 (2020).
19. Xiaodong Yan, Mupeng Zheng, Yudong Hou, and Mankang Zhu, *J. Eur. Ceram. Soc.* **37**, 2583 (2017).
20. H. Kaddoussi, A. Lahmara, Y. Gagoua, B. Manoun, J. N. Chotard, J. -L. Dellis, Z. Kutnjak, H. Khemakhem, B. Elouadi, and M. El Marssi, *J. Alloys Compd.* **713**, 164 (2017).
21. Jie Liu, Bin Yang, Lijun Lu, Xiaolin Wang, Xiuyan Li, Xiang Chen, and Jingquan Liu, *Sens. Actuator A Phys.* **303**, 111796 (2020).
22. Kwanlae Kim, *Korean J. Met. Mater.* **57**, 38 (2019).
23. Kyoung-Seok Moon, Seong Eun Lee, and Jun-Hyeong Kwon, Enhancement of Dielectric Properties via Crystal Structure and Microstructure Control in the (K0.5Na0.5)NbO3-SrTiO3 System, *Korean J. Met. Mater.* **59**, 499 (2021).